ADVANCED MATERIALS

Two-Photon Photographic Production of Three-Dimensional Metallic Structures within a Dielectric Matrix**

By *Pu-Wei Wu*, *Wei Cheng*, *Ignacio B. Martini*, *Bruce Dunn*,* *Benjamin J. Schwartz*, and *Eli Yablonovitch*

Two-photon processes have been used to create a number of chemical or physical processes including optical data storage,[1] fluorescence imaging,[2] optical waveguiding,[3] and lithographic fabrication.[4,5] Advances associated with the latter have become very impressive as three-dimensional optical circuitry[6] and photonic bandgap structures[7] show the promise of using two-photon or higher-order multiphoton processes for fabricating complex three-dimensional structures. The appeal in using multiphoton processes for three-dimensional fabrication of materials is that with the nonlinear dependence on intensity, the absorption of light is highly localized in a small volume near the focal region. In addition, because of the low linear absorption of dielectric materials in the near-IR, the use of high peak-power light at these wavelengths allows for deep penetration into the interior of the material. The technology for using two-photon processes has been advanced further by the development of photosensitive initiators[7] and the availability of commercial laser systems in which single-shot, two-photon exposures allow three-dimensional structures to be constructed at MHz repetition rates.[8] While two-photon lithography has been used successfully for producing polymeric structures, the development of this approach for fabricating three-dimensional metallic structures has not been reported.

In this communication, we demonstrate the lithographic fabrication of a three-dimensional metallic structure based on a three-step photographic-type approach. First, multiphoton exposure to femtosecond laser radiation creates a three-dimensional latent image; this image becomes a three-dimensional structure during a second, development process. A final fixing step then retains the object. The ability to lithographically fabricate metals using writing methods similar to those demonstrated with polymers is likely to initiate opportunities in three-dimensional wiring for microelectronics as well as metallodielectric structures for microelectromechanical (MEMS) and photonic bandgap applications.

[*] Prof. B. Dunn, Dr. P.-W. Wu, W. Cheng
Department of Materials Science and Engineering
University of California, Los Angeles
Los Angeles, CA 90095-1595 (USA)
E-mail: bdunn@ucla.edu
Dr. I. B. Martini, Prof. B. J. Schwartz
Department of Chemistry and Biochemistry
University of California, Los Angeles
Los Angeles, CA 90095-1569 (USA)
Prof. E. Yablonovitch
Electrical Engineering Department
University of California, Los Angeles
Los Angeles, CA 90095-1594 (USA)

[**] This material is based upon work supported by, or in part by, the US Army Research Office/DARPA under contract number DAAG55-97-1-0384.

The photographic medium used in these experiments consists of a liquid phase immobilized in the pores of a SiO_2 matrix prepared by the sol–gel process.[9] Different silver salt solutions comprise the liquid phase; these solutions were chosen on their ability to form either a stable latent image for the exposure process, or to precipitate silver as required in the development process. The interconnected porous network developed in the sol–gel process enables the initial pore liquid to be replaced with other solutions as desired.

The photographic medium was prepared by mixing a 1:2 weight ratio of hydrolyzed silica sol with deionized (DI) water. The hydrolyzed sol was prepared by ultrasonic mixing of tetramethoxy silane (TMOS; $Si(OCH_3)_4$) and H_2O with an acid catalyst (H_2SO_4 or HNO_3) for 15 min (molar ratio: $TMOS/H_2O/H^+ = 1:2:7 \times 10^{-5}$). The sol–water mixture formed a homogeneous solution and was poured into a methacrylate cuvette and sealed with Parafilm. Gelation occurred in approximately 2 h. At this stage the material is considered to be a "wet gel", which consists of a highly porous oxide matrix of SiO_2 in which the pores are filled with solvent. The SiO_2 phase that forms from the hydrolysis and condensation reactions is approximately 5 vol.-%. The pore diameters are in the range of 200 Å and are interconnected in a three-dimensional network.[10] Because of this interconnected morphology, it is possible to replace the solvent phase present in the pores by simply immersing the gel in the desired solution. The use of solvent exchange to alter the chemistry of the pore liquid has been well documented and is the basis for using sol–gel glasses as chemical sensors.[11,12]

The preferred solvent phase for forming the latent image is an aqueous solution of $AgNO_3$. To incorporate this solution in the matrix, the initial wet gel is first immersed in a large excess of DI water several times to wash out any pore solvents. The washed gels are then immersed in a 1.06 M $AgNO_3$ aqueous solution in a second solvent exchange step. Since the gels are placed in tightly covered cuvettes, they exhibit no shrinkage as would normally occur during solvent loss. The material is stable to room temperature and ambient lighting conditions.

The latent image is produced using a regeneratively amplified Ti:Sapphire laser. The laser system produces ~120 fs transform-limited pulses centered at 800 nm with 1 mJ of energy at a 1 kHz repetition rate. Control of pulse energy was achieved by attenuation with calibrated neutral density filters. Pulse widths were measured with a single-shot autocorrelator. For the experiments reported here, we chose a long focal length lens (1 m) which focuses the laser pulses to a $\sim 100 \times 120$ μm spot at a fixed position.[13] The wet gel (i.e., the photographic medium) is placed in a sample holder and drawn past the focused spot quickly enough so that each pulse from the laser impinges on a fresh spot of the wet gel.[8] The long focal volume produced by the 1 m focal length lens allows multiphoton exposure of the wet gel to occur over a significant fraction of its 1 cm thickness. Thus, each of these scans produces a series of yellow lines (exposures) that penetrate through the entire sample. The experimental configuration for the scans and some of the resulting images are shown in Figure 1a and 1b.

  0935-9648/00/1910-1438 $ 17.50+.50/0

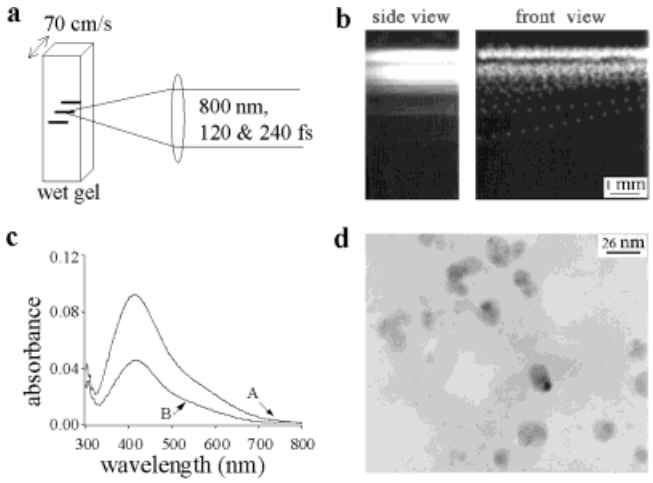

Fig. 1. Latent image formation in sol-gel samples solvent exchanged with $AgNO_3$ solution. a) Schematic of the arrangement for the laser exposure. b) Optical photographs for the front and side views of a sol–gel sample after laser irradiation (intensity of 13.9 TW/cm^2 with fluence of 1.67 J/cm^2 pulse). The top of the sample was exposed to repetitive scans. The lower part of the cuvette shows exposures to single scans. The magnification of these photographs is 5×. c) Absorbance curves for the wet gel samples exposed to different laser intensities. (curve A = 5.6 TW/cm^2 pulse; curve B = 2.8 TW/cm^2 pulse). In both cases, the background absorbance for an unexposed sample was subtracted. A silver plasma resonance peak, not present prior to irradiation is clearly evident after irradiation. d) TEM photomicrograph showing the sol–gel sample after laser exposure at an intensity of 13.9 TW/cm^2 with fluence of 1.67 J/cm^2 pulse. Samples were prepared as powders and suspended in methanol. After sonication, the solution was dipped onto a copper TEM grid.

The latent images were characterized using optical absorption spectroscopy, transmission electron microscopy (TEM), and optical photography. The yellow color produced by laser exposure is the result of a broad optical absorption band at ~410 nm, which arises from the surface plasmon excitation of nanometer-size silver particles (Fig. 1c, curve B).[14] The breadth of the absorption peak is from a fairly wide particle size distribution as well as a varying aspect ratio for the silver particles; one can estimate the average particle size to be in the range of 5 to 20 nm.[14] The use of higher intensity pulses (Fig. 1c, curve A) produces a stronger absorption, indicating that a greater number of silver particles are being produced. The TEM results (Fig. 1d) are consistent with the optical absorption spectra: the region within a given focused beam spot is shown to consist of silver nanoparticles with sizes primarily in the range of 5 to 20 nm.

Optical photographs of the wet gel (in its cuvette) show the nature of the latent image patterns produced by laser exposure (Fig. 1b). Towards the top of the cuvette, the visible image is enhanced by repetitive scans within a 3 mm band. Approximately 4000 exposures were made within this band. Each exposure produces a single image line extending throughout the sample as evident from the side view of the cuvette. Figure 1b also shows that single scans are able to produce an image, although the contrast is not as pronounced. For the single scans, the exposures are made at a slight angle to better resolve the individual lines. These images demonstrate that a single laser pulse produces an individual line of Ag nanoparticles penetrating through the gel. The diameter of this line is approximately 150 μm, with the exact diameter depending on the laser intensity. The observed image size is consistent with the 100 × 120 μm diameter beamwaist at the focus. For a single 120 fs laser pulse, we can place an upper limit for the threshold fluence = 0.668 J/cm^2 pulse (I = 5.568 TW/cm^2 pulse): the threshold fluence (and intensity) we report for observing an image is limited by our ability to measure the optical absorption of a small number of Ag nanoparticles in a ~100 μm exposed spot.[13] Laser damage of the cuvette did not occur until the fluence exceeded ~1.7 J/cm^2 pulse, while damage of the wet gel occurred at somewhat higher levels than this. The relatively low threshold fluence verifies that Ag particle production results from a multiphoton absorption process and not from ablation or damage of the wet gel. The factor of 2.5 difference between the latent image and damage thresholds provides an adequate range for image formation without laser damage.

A series of control experiments can be used to verify that the process that produces the latent image is at least two-photon in nature. First, no evidence was found for Ag production following exposure of the $AgNO_3$-impregnated wet gels to continuous radiation, either at 800 nm from a continuous wave (CW) laser or at 266 nm from a Hg arc lamp. This is consistent with the idea that the high intensities associated with multiphoton processes are necessary to nucleate the Ag nanoparticles that grow to form the latent image. This idea was tested in a second series of measurements that utilized femtosecond laser pulses chirped by intentional misalignment of the compressor optics after the regenerative amplifier. The gel samples were exposed to both transform-limited (120 fs) and temporally stretched (240 fs) light pulses of the same energy and spot size (fluence). If image formation results from multiphoton absorption, exposures by pulses with the same fluence (J/cm^2) but twice the pulse width should decrease the number of Ag nanoparticles formed. The results shown in Figure 2 indicate that by using longer pulses, the intensity of the Ag plasmon absorption comprising the latent image, which is directly proportional to the number of Ag nanoparticles produced by exposure, does decrease with decreasing excitation intensity even though the fluence is constant. Thus, all the available evidence suggests that the production of the latent image relies on a two- (or higher) photon process.

Another feature evident from Figure 2 is that the magnitude of the decrease in Ag production is not the factor of four

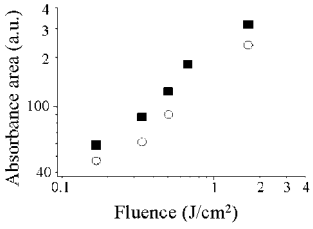

Fig. 2. The effect of pulse width on latent image. Gel samples were exposed to 120 fs (■) and 240 fs (○) pulse widths. The area under the plasma absorption band is used to characterize image size.

  0935-9648/00/1910-1439 $ 17.50+.50/0

ADVANCED MATERIALS

that is expected for two-photon absorption but is instead only between 1.5 and 2. The less steep power dependence is the sign of a multiphoton process near saturation, and thus we are unable to conclude definitively as to whether the exposures are two-photon in nature or result from a higher order process. It is certainly possible, for example, that laser-induced ionization of the pore solvent contributes to production of the latent image. The dielectric breakdown of water occurs from the high electric fields generated from short laser pulses.[15] Although the threshold intensity for breakdown of water is a function of pulse width and beam size, it generally falls within the range of 0.01 to 0.6 TW/cm^2 pulse. Since this value is lower than the typical intensity used in the laser patterning experiments, it is possible that electrons freed from the ionization process are able to reduce the dissolved silver ions. Whether this type of indirect reduction mechanism is the dominant one or competes with direct multiphoton absorption by Ag ions, the multiphoton nature of the process ensures that it is possible to use high numerical aperture objectives to expose only the interior of the impregnated gels, allowing latent images to be written in three dimensions.

Once the latent Ag-particle images are written, development of the images is based on the reduction of an aqueous $AgClO_4$ solution contained in the pores of the laser-exposed wet gel. After laser exposure, the wet gels were first washed with excess water to remove the encapsulated $AgNO_3$ solution and then immersed in a solution of 0.49 M $AgClO_4$ in a second solvent exchange treatment. These gels were kept in the $AgClO_4$ solution as they were annealed at 60–80 °C for an extended period of time (up to 80 h). This development process takes advantage of the reactivity of $AgClO_4$. Previous work has shown that reduction to form Ag particles occurs in aqueous $AgClO_4$ solutions upon irradiation by ^{60}Co γ-rays,[16] and that the yield is enhanced in concentrated solutions. In the present case, thermal treatments (with perhaps some contribution from ambient UV) enable the reduction to proceed at a relatively slow rate. The reduction of the $AgClO_4$ solution caused the yellow latent images to become substantially darker, but did not lead to darkening of the background, which would reduce image contrast. Once developed, the images are then fixed by a final solvent exchange step with water to remove the $AgClO_4$ solution.

The image darkening that occurred during the development process was monitored using in situ optical absorption. The developing images continued to display the characteristic 410 nm Ag plasmon absorption band, but now with the band increasing in intensity and breadth upon development, indicating that larger silver particles are present at higher concentration. TEM of the microstructure shows that the majority of the Ag nanoparticles have grown to the 40–50 nm range after development and that most of the smaller particles have disappeared.

X-ray diffraction (XRD) taken on gel samples after the development process indicates that silver is produced. As in conventional photography, it is possible to overdevelop a sample and this can be accomplished by leaving the gel samples in the developing solution for ~80 h. The X-ray pattern for this sample consists of the strongest peaks for silver superimposed on the characteristically broad peaks arising from the amorphous sol–gel matrix (Fig. 3a). A development time of 80 h is not usable for our purposes, however, because darkening of the

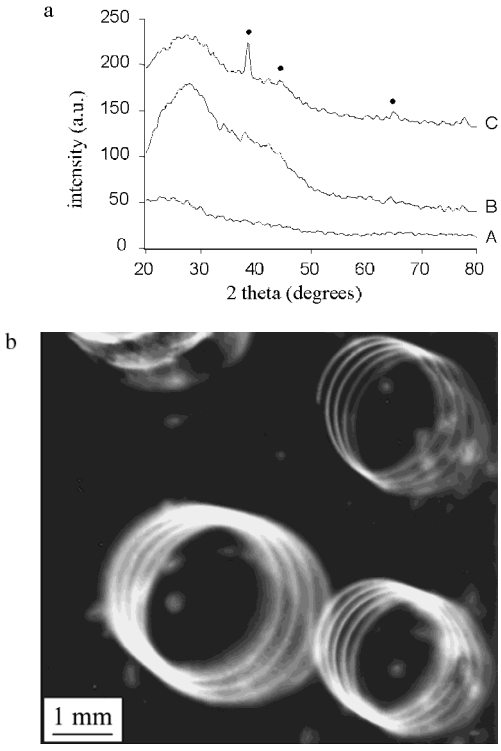

Fig. 3. Silver formation within sol–gel materials. a) XRD pattern for gel samples subjected to different development times after laser exposure at an intensity of 5.6 TW/cm^2. A) no treatment, B) 36 h development time, and C) 80 h development time. The pattern in C is identified as the silver cubic phase with peaks indexed for the (111), (200), and (220) planes. b) Three-dimensional spiral structure produced within silver-doped sol–gel materials. The latent image was produced using multiple pulse exposures with an energy of 60 μJ per pulse (800 nm, 120 fs pulse) using a 25 mm focusing lens. The development time was 8 h.

background due to spontaneous Ag precipitation in regions where there was no latent image substantially reduces the contrast. Empirically, we found that a development time of 36 h produces images with the best contrast.

The ability to use this photographic-like process to develop a macroscopic three-dimensional structure is shown in Figure 3b. The wet gel (containing the $AgNO_3$ solution in its pores) was laser irradiated at a fixed position in space using a short (25 mm) focal length lens. The short focal length lens and the multiphoton nature of the exposure process allowed Ag nanocrystals to be written only in the interior of the wet gel,[7,8] rather than in a line throughout the wet gel as with the 1 m lens. The gel was placed on a rotation stage whose axis was aligned slightly off-center from the position of the laser spot. Simultaneous translation and rotation of the wet gel during laser exposure thus allows spiral objects to be written in a single fabrication step. The latent spiral image was then developed with the $AgClO_4$ treatment and fixed by solvent exchange in water.

  0935-9648/00/1910-1440 $ 17.50+.50/0

In summary, we have demonstrated a photographic-like approach for producing three-dimensional silver structures. Fabrication is based on the formation of a latent image defined by laser irradiation. Multiphoton processes are involved in image formation, allowing features to be written directly into the interior of the matrix in a single fabrication step. Development of the image is accomplished from the controlled reduction of a $AgClO_4$ solution. Although the final microstructure is composed of discrete, 40–50 nm diameter silver particles, we are presently exploring new development methods that enable the particles to become interconnected over longer distances, leading to the lithographic patterning of metal wires in three dimensions in the interior of the gel. We expect that the ability to lithographically produce three-dimensional metallic structures should be compatible with recently developed three-dimensional polymer fabrication processes, thus greatly extending the opportunities for lithographic microfabrication.

Received: March 6, 2000
Final version: June 9, 2000

[1] D. A. Parthenopoulos, P. M. Rentzepis, *Science* **1989**, *245*, 843.
[2] W. Denk, J. H. Strickler, W. W. Webb, *Science* **1990**, *248*, 73.
[3] S. J. Frisken, *Opt. Lett.* **1993**, *18*, 1035.
[4] E. S. Wu, J. H. Strickler, W. R. Harrell, W. W. Webb, *Proc. SPIE* **1992**, *1674*, 776.
[5] S. Maruo, O. Nakamura, S. Kawata, *Opt. Lett.* **1997**, *22*, 132.
[6] M. P. Joshi, H. E. Pudavar, J. Swiatkiewicz, P. N. Prasad, B. A. Reianhardt, *Appl. Phys. Lett.* **1999**, *74*, 170.
[7] B. H. Cumpston, S. P. Ananthavel, S. Barlow, D. L. Dyer, J. E. Ehrlich, L. L. Erskine, A. A. Heikal, S. M. Kuebler, I.-Y. S. Lee, D. McCord-Maughon, J. Qin, H. Rockel, M. Rumi, X.-L. Wu, S. R. Marder, J. W. Perry, *Nature* **1999**, *398*, 51.
[8] G. Witzgall, R. Vrijen, E. Yablonovitch, V. Doan, B. J. Schwartz, *Opt. Lett.* **1998**, *23*, 1745.
[9] C. J. Brinker, G. W. Scherer, *Sol–Gel Science*, Academic, San Diego, CA **1990**.
[10] J. H. Harreld, W. Dong, B. Dunn, *Mater. Res. Bull.* **1998**, *33*, 561.
[11] D. Avnir, S. Braun, O. Lev, M. Ottolenghi, *Chem. Mater.* **1994**, *6*, 1605.
[12] B. Dunn, J. I. Zink, *Chem. Mater.* **1997**, *9*, 2280.
[13] The large spot size was chosen both to allow easy detection of the latent image, and to facilitate characterization of the image formation process by optical spectroscopy and TEM.
[14] U. Kreibig, M. Vollmer, *Optical Properties of Metal Clusters, Springer Series in Materials Science*, Vol. 25, Springer, New York **1995**.
[15] C. A. Sacchi, *J. Opt. Soc.Am. B* **1991**, *8*, 337.
[16] G. Czapski, A. O. Allen, *J. Phys. Chem.* **1966**, *70*, 1659.

A Novel Route for the Preparation of Nanocomposite Magnets**

By *Xiangyi Zhang*,* *Jinwu Zhang*, and *Wenkui Wang*

Nanocomposite magnets consisting of a two-phase distribution of hard and soft magnetic grains have attracted considerable interest since they could, by exchange coupling,[1] potentially provide a maximum energy product, $(BH)_{max}$, in excess of 100 MGOe,[2] which is much larger than the theoretical limited value of anisotropic Nd–Fe–B sintered magnets, 64 MGOe. Moreover, the nanocomposite magnets are of commercial interest because they require less of an expensive rare earth element. The nanocomposite magnets have been mainly fabricated by rapid quenching and subsequent annealing, direct melt spinning, or mechanical alloying. Although the exchange coupling between hard and soft magnetic phases enhances remnant magnetization above the value expected for isotropic single-phase hard magnets, the Stoner–Wohlfarth value of 0.5 Ms, at present the maximum energy product of practical nanocomposite magnets, 10–20 MGOe, is still significantly lower than that predicted by theory. The basic cause has been attributed by most scientists working in the field to the difference in the microstructure parameters between practical nanocomposite magnets and the theoretical model.[3–6] Recently, micromagnetic calculations have attracted more attention in order to understand the basic mechanisms that determine the magnetic properties of the nanocomposite magnets and provide some guidelines for optimizing the microstructure of the magnets.[7–11] Calculation results have shown that the maximum energy product of nanocomposite magnets is strongly dependent on their microstructure parameters, grain size, the ratio of volume fraction between soft and hard magnetic phases, phase distribution, and grain boundaries. Schrefl et al. have reported[7] that it should be possible to substantially increase the maximum energy product (>80 MGOe) in nanocomposite magnets by reducing the grain size of isotropic nanocomposite magnets to less than 10 nm and controlling the ratio of volume fraction between soft and hard magnetic phases at a proper value. However, the practical preparation of such a microstructure required by the theoretical model, especially the fine grain size below

[*] Dr. X. Zhang,[+] Dr. J. Zhang, Prof. W. Wang[++]
College of Materials Science and Engineering, Yanshan University
Qinhuangdao 066004 (P. R. China)
E-mail: xiangyi@itap.physik.uni-stuttgart.de
[+] Present address: Institut für Theoretische und Angewandte Physik, Universität Stuttgart, Pfaffenwaldring 57 / V1, D-70550 Stuttgart, Germany.
[++] Present address: Institute of Physics, Chinese Academy of Sciences, Beijing 100080, P. R. China.

[**] This work is supported by Chinese National Nature Science Foundation under grant no. 19974035 and Nature Science Foundation of Hebei Province of People's Republic of China under grant no. 599240. Dr. X. Y. Zhang thanks the Alexander von Humboldt Foundation and the help given by Dr. W. Sprengel and Prof. H.-E. Schaefer of Stuttgart University, Germany.

  0935-9648/00/1910-1441 $ 17.50+.50/0